

From jamming to collective cell migration through a boundary induced transition

Oleksandr Chepizhko,¹ Maria Chiara Lionetti,² Chiara Malinverno,^{3,4}
Giorgio Scita,^{3,4} Stefano Zapperi,^{5,6,7} and Caterina A. M. La Porta²

¹*Institut für Theoretische Physik, Leopold-Franzens-Universität Innsbruck,
Technikerstrasse 21a, A-6020 Innsbruck, Austria*

²*Center for Complexity and Biosystems,
Department of Environmental Science and Policy,
University of Milan, via Celoria 26, 20133 Milano, Italy*

³*IFOM, the FIRC Institute of Molecular Oncology,
Via Adamello 16, 20139 Milano, Italy*

⁴*Dipartimento di Scienze della Salute, San Paolo,
University of Milan, 20122 Milano, Italy*

⁵*Center for Complexity and Biosystems,
Department of Physics, University of Milano,
via Celoria 26, 20133 Milano, Italy*

⁶*CNR - Consiglio Nazionale delle Ricerche,
Istituto per l'Energetica e le Interfasi,
Via R. Cozzi 53, 20125 Milano, Italy*

⁷*Department of Applied Physics, Aalto University,
P. O. Box 11100, FIN-00076 Aalto, Espoo, Finland*

Abstract

Cell monolayers provide an interesting example of active matter, exhibiting a phase transition from a flowing to jammed state as they age. Here we report experiments and numerical simulations illustrating how a jammed cellular layer rapidly reverts to a flowing state after a wound. Quantitative comparison between experiments and simulations shows that cells change their self-propulsion and alignment strength so that the system crosses a phase transition line, which we characterize by finite-size scaling in an active particle model. This wound-induced unjamming transition is found to occur generically in epithelial, endothelial and cancer cells.

I. INTRODUCTION

Understanding collective cell migration, when cells move as a cohesive and coordinated group is important to shed light on key aspects of embryogenesis, wound repair and cancer metastasis [1]. While cellular and multicellular dynamics and motility is controlled by a complex network of biochemical pathways [2], it is becoming increasingly clear that a crucial role is also played by physical interactions among cells and between cells and their environment[3–7]. Dense cellular assemblies, such as epithelial monolayers or cancer cell colonies, share many features with amorphous glassy materials, displaying slow relaxation[8], jamming [9] and intermittent avalanche fluctuations [10].

Cells can collectively flow like a fluid, but as cell proliferation increases cell density mutual crowding leads to slowing down and arrest [8, 9]. The phenomenon of cell jamming could have a functional biological role, ensuring the development of tissue elasticity and protective barriers in epithelial tissues, providing also a suppressive mechanism for the aberrant growth of oncogenic clones. An unjamming transition into a collective flowing state could also provide a mechanism for cell migration that is alternative to the well studied epithelial-to-mesenchymal transition (EMT), characterized by individual cell migration as a result of the loss of intracellular adhesion [11].

The loss of motility in cellular assemblies shares similar features to the jamming transition observed in disordered materials such as colloids, granular media or foams [12]. As in disordered solids, cell jamming is thought to occur across different routes, either through the increase of cell density, or the reduction of the active forces responsible for cell motility. In analogy with inanimate glassy systems, it seems reasonable to assume that jamming could also be produced by increasing intracellular adhesion, yet experimental observations show that unjamming is associated with an increased adhesion, questioning the role of adhesion as a principal determinant of jamming [9]. Recent experiments also show that over-expression of the endocytic master regulator RAB5A leads to rapid fluidization and unjamming of a jammed confluent cell monolayer, due to polarization of cell protrusion and increase in traction force [13].

Theoretical understanding of the cell jamming transition mostly relies on simulations of vertex models [14], similar to those used for foam rheology [15, 16], and self-propelled Voronoi (SPV) models [17, 18], also including self-propulsion typical of active particle models[19–22].

In the SPV model, space is subdivided into Voronoi polygons endowed with a mechanical energy due to cell surface tension, compression and adhesion. The polygonal structure then evolves according to equation of motion taking into account an active self-propulsion force and a noise term. Extensive numerical simulations allow us to identify the jamming transition and to reconstruct a possible phase diagram in terms of the main physical parameters encoded in the model [18]. In this way, it is possible to identify physical determinants for jamming, including the strength of the self-propulsion force and the shape anisotropy of the cell, determined by the ratio between the cell area and its squared perimeter [9, 18].

While cell jamming is typically observed experimentally by following in time the evolution of a cell monolayer in a confined space, collective cell migration is mostly observed and quantified in wound healing assays where cells are allowed to invade an empty space [3–7, 20–22]. The implementation of current vertex and Voronoi models rely on periodic boundary conditions and are thus not appropriate to study wound healing, whose statistical features are well described by active particle models [10, 19, 21]. In this paper, we analyze the response of a jammed cell monolayer to the appearance of a wound, which creates empty space for the cells at the boundary. To this end, we analyze a large set of time-lapse images of cell layers using different cell types and experimental treatment, under confluent and wound healing conditions, and compare the results with simulations of an active particle model. We show that the model is able to quantitatively describe experimentally measured velocity distributions with open but also with confined boundary conditions. The model allows for a systematic investigation of the role of each relevant physical parameter so that we can place each experiment into a suitable phase diagram. Our simulations show that the model exhibits a clear jamming transition characterized by finite-size scaling. When we compare wound healing with confined experiments, we find that the latter are described by a set of physical parameters that place the system into the jamming phase, while the former fall into the flowing phase. Hence, the presence of a wound re-awakens jammed cells in a way similar to the effect of the overexpression of the endocytic regulator RAB5A [13].

II. EXPERIMENTAL RESULTS

We consider time lapse images recorded during wound healing assays performed for a variety of cell lines under different experimental conditions (see section A for detailed infor-

mation): HeLa cells on different substrates: plastic, soluble collagen, or fibrillar collagen (see [10]); Endothelial cells derived from embryonic stem cells with homozygous null mutation of the VE-cadherin gene (VEC null) [23] and those with the corresponding wild type form of VE-cadherin (VEC positive) [24]; Endothelial cells isolated from lungs of wild type adult mice (lung ECs) [10, 25]; A non-tumorigenic human mammary epithelial cell line (MCF-10A) with the over-expression of RAB5A, known to induce unjamming, and the corresponding wild type (WT) cells [13]. As a comparison, we also analyze HeLa cells and MCF-10A cells in confluent conditions without inducing wound healing.

We analyze all the experimental time lapse images using particle image velocimetry (PIV) which allows us to estimate the local velocity field inside the cell sheet (See Fig. 1a) and the corresponding velocity distributions [10]. In particular, we measure the distribution of the velocity absolute values $P(v)$ (See Fig. 1b), the distribution of the velocity orientations (See Fig. 1c) and the velocity-velocity correlation lengths ξ from an exponential fit of the correlation functions (See Fig. 1c). It is interesting to notice that correlations lengths obtained from MCF-10A cells under different conditions scale linearly with the standard deviation of the velocity distribution $\Sigma = \sqrt{\langle(v_x^2 + v_y^2)\rangle - (\langle v_x \rangle)^2 - (\langle v_y \rangle)^2}$. This relation was predicted by a theoretical model of collective cell migration where it implies that the effective friction is dominated by cell-cell interactions over cell-substrate interactions [26].

Considering all the experimental results, we obtain a set of 40 distributions for different cell lines and experimental conditions describing the statistical features of the velocity during collective cell migration. To visualize all the data in a simple way, in Fig. 3a we report the average velocity $\langle v_x \rangle$ perpendicular to the front as a function of Σ . The results show that the standard deviation of confluent systems is roughly one order of magnitude smaller than the one observed during wound healing for the same cells. Considering the wound healing case, we observe that MCF-10A cells move considerably faster than the other cells and, as expected, RAB5A overexpression leads to net increase in the average velocity with little changes in Σ .

III. MODEL

In order to relate the statistical properties of collective cell migration quantified from our experiments with the presence of a jamming critical point, we compare the experimental

results with simulations of a model for interacting cells similar to the one introduced in Ref. [21]. Cells are treated as particles moving according to the following equation of motion:

$$\frac{d\mathbf{v}_i}{dt} = -\alpha\mathbf{v}_i + \sum_{j:n.n.of\ i} \left[\frac{\beta}{N_i}(\mathbf{v}_j - \mathbf{v}_i) + \mathbf{f}_{ij} \right] + \sigma\boldsymbol{\eta}_i + \hat{\mathbf{v}}F_0. \quad (1)$$

The first term represents the dissipation processes and α is a damping parameter. The second term represents the interaction of i -th cell with the other cells. The interaction reflects the tendency of a particle to orient its velocity with the velocity of its neighbors, with a coupling strength β , and N_i is the number of neighbors of i -th cell. The second interaction term, \mathbf{f}_{ij} , represents the short-range hard-core repulsion and long-range attraction, and has the form

$$\mathbf{f}_{ij} = -\nabla_i U(r_{ij}), \quad (2)$$

where

$$U(r) = U_0 \exp(-(r/a_0)^2) + U_1(r - a_1)^2 H(r - a_1), \quad (3)$$

where $H(x)$ is the Heaviside function $H(x) = 1$ for $x > 0$ and $H(x) = 0$ otherwise. The motion of a cell is affected by a noise term $\sigma_0\boldsymbol{\eta}_i$, where $\boldsymbol{\eta}_i$ is an Ornstein-Uhlenbeck process with correlation time τ :

$$\tau \frac{d\boldsymbol{\eta}_i}{dt} = -\boldsymbol{\eta}_i + \boldsymbol{\xi}_i, \quad (4)$$

$\boldsymbol{\xi}_i$ is a delta-correlated white noise, independent for each cell $\langle \boldsymbol{\xi}_i(t)\boldsymbol{\xi}_j(t') \rangle = \delta_{ij}\delta(t - t')$.

As in the original model [21], the free surface is modeled by surface particles, that are hindering cells invade the space. The interaction between a surface particle and a cell is modeled by:

$$\mathbf{f}_{ij}^s = -\nabla_i U^s(r_{ij}), \quad (5)$$

where $U^s(r)$ is $U^s(r) = A_s \exp(-(r/a_s)^2)$. With each surface particle a scalar damage variable q is associated, and it is chosen to obey:

$$\nu \frac{dq_i}{dt} = \sum_{j:\mathbf{r}_j \in S_i} |\mathbf{f}_{ij}^s|. \quad (6)$$

The surface particle disappears if the damage variable reaches its critical value $q_i = q_c$. To simulate wound healing conditions, we place the cell in a box of size $2L \times L$ in which we place cells surrounded by surface particles. We first do not allow damage on the surface particles and let the system relax for a time $T/4$. We then allow surface particles to be damaged so

that the wound healing process starts. We first let the front evolve for an additional time $T/4$ and finally collect velocity statistics for a time $T/2$. This procedure allows to minimize transient effects. The model can also be simulated in confluent conditions by setting the damage variable to $q_c = \infty$, so that the cells never invade the surrounding space.

IV. SIMULATIONS

A. Experimental velocity distribution are described by the model

To compare the experiment with the model, we run a large set of simulations with both open and closed boundary conditions, employing a cell density that corresponds to the one observed in experiments for confluent cell layers. We explore the parameter space defined by different values of $(F_0, \sigma_0, \beta, \alpha, U_1)$ and inspect how each parameter affects the velocity distributions (see Fig. 2). We observe that F_0 and α have a considerable effect on $\langle v_x \rangle$, while β and σ_0 have opposite effects on the velocity fluctuations: Σ increases with σ_0 and decreases with β . The adhesion strength is found to have little effect on the velocity distributions for the range we examined.

We find the best match between experiments and simulations (see supplementary methods) and identify a set of four parameters $(F_0, \sigma_0, \beta, \alpha)$ that best describe each individual experiment. Representative examples of the good match between experiments and model are reported in Fig. 1 for the case of MCF-10A cells under different conditions. We have also checked that the simulations reproduce the value of the correlation length with reasonable accuracy. The collection of parameters obtained for all the experiments is summarized in Fig. 3b as normalized color maps. The map allows us to observe some general trends in the parameter space: in particular MCF10-A with RAB5A overexpression stand out for their higher value of self-propulsion (F_0) and mutual alignment (β) with respect to the other cells. Furthermore, MCF-10A, both WT and RAB5A, display weaker noise (σ_0) in comparison with the other cells.

B. Finite size scaling at the jamming transition

A simple inspection of the experimentally measured velocity distributions does not provide a clear understanding of the possible jamming or flowing behavior of the cell monolayer.

ers. Simulating the model, however, allows for a complete characterization of its dynamical behavior in term of a reduced set of parameters. Following recent work, we analyze the mean-square displacement (MSD) of individual cells in simulations of confluent layers and study how it changes as key parameters are varied. For instance, Fig. 4a shows that the MSD is a linear function of time whose slope, the effective diffusion constant D , increases with noise parameter σ_0 . A sharp increase in D is usually associated with a transition from a jamming to a flowing state. In our case, Fig. 4b shows that D depends on σ_0 in a system-size dependent manner. This is generally expected for phase transitions in and out of equilibrium, where finite size scaling governs the behavior of the system near the critical point. We thus propose a finite-size scaling form for the noise and size dependence of the diffusion constant

$$D(\sigma_0, N) = f((\sigma_0 - \sigma_c)N^{1/\nu}) \quad (7)$$

where the scaling function $f(x) \propto x^\gamma$ for $x > 0$ and $f(x) = \text{const.}$ for $x < 0$. The data collapse reported in Fig. 4c according to Eq. 7 indicates that $1/\nu = 0.5$ and $\gamma = 0.85$. A similar finite-size scaling collapse can be done in dependence on F_0 : $D(F_0, N) = g((F_0 - F_c)N^{1/\nu'})$, with $g(x) \propto x^{\gamma'}$ for $x > 0$ (see Fig. 5), yielding $1/\nu' = 0.5$ and $\gamma' = 1.3$.

C. Wound healing induces unjamming

Collecting together all the simulations performed, we construct a phase diagram distinguishing the jammed from the flowing state as a function of F_0 and σ_0 , as reported in Fig. 6. Here for practical reasons, we have concentrated on fixed values for $\beta = 10$ and $\alpha = 1.4$ that correspond to a large set of experimental data. It is possible in principle to reconstruct the whole 4-dimensional phase diagram but this is extremely demanding computationally.

We are now in position to reach the goal posed at the beginning of this paper and identify the phase for each experimental sample. To this end, we report in Fig. 6 all the parameter values (F_0, σ_0) extracted from the experimental measurement (see Table S1 for the parameter list). The general trend we observe from the figure is that all the experiments performed in confluent layers fall into the jammed phase, while almost all of the wound healing experiments are in the flowing phase. Notice that here we are projecting all the data into the $(\beta = 10, \alpha = 1.42)$ plane so discrepancies could also arise due to the fact that experimental data are described by different values of β and α .

Taken together our results suggest that when a jammed confluent layer is perturbed by wound healing, providing additional space for the cells, the system undergoes a phase transition to the flowing state. This is reflected by the fact that key parameters describing self-propulsion, noise or alignment change their values, implying that the monolayer responds in an active way to the change of boundary conditions. We checked that this process is not an artifact of the model or the fitting by considering wound healing before and after closure. Results show that it is possible to fit the velocity distributions before and after healing with the same parameters. It is only some time after closure that the cell layer slowly falls back into the jammed state.

V. DISCUSSION

Soft and glassy materials are known to undergo a jamming transition, characterized by limited mobility and slow relaxation upon fine tuning of a set of physical control parameters including density, temperature and shear stress [12]. Dense cellular assemblies such as epithelial tissues and cancer are recently emerging as paradigmatic examples of jamming in active matter [9, 26, 27], a well studied non-equilibrium state of matter where an internal force drives each of the elementary units of the system. Examples of active matter range from artificial self-propelled colloidal particles, to bacteria, epithelial and cancer cells or even large groups of animals such as fish schools or birds flocks. A key issue for active matter is to understand what are the main physical determinants for jamming, which would play a role analogous to stress, density and temperature in conventional matter.

Current understanding of the jamming transition in cellular systems comes mostly from vertex models [14] and SVP models [17, 18], which allow to clarify the role of many key biophysical parameters, such as cell anisotropies and self-propulsion strength. These models, however, are defined for systems with periodic boundary conditions and are therefore not appropriate to study the response of jammed epithelia to a wound, a well studied protocol to understand and quantify collective cell migration in epithelial and cancer cells [3–7, 10, 20–22]. Active particle models have proven very effective to quantitatively describe wound healing [10, 21], but are usually not employed to study the jamming transition. Hence, the relation between wound healing and the jamming transition has not been explored. In the paper, we fill this gap by a combination of experiments and numerical simulations.

We analyze a large set of time-lapse experiments of cellular assemblies performed for different cell lines both in confluent conditions or after wound healing. In all these case, we compute the velocity distributions by PIV and study how the distribution changes in presence of a wound. We start our analysis from the MCF-10A cell line that was recently shown to undergo a transition from a jammed to a flowing state by over-expression of RAB5A, a master regulator of endocytosis [13]. Here we compare this transition with the similar fluidization induced by a wound. To obtain a quantitative characterization of the transition, we compare the experimental results with numerical simulations of an active particle model. In this way, we obtain the model parameters that best describe the experimentally measured velocity distributions. This parameters describe the self-propulsion force, the alignment interactions, intracellular adhesion, damping and noise and allow for a physical characterization of different cell lines and experimental conditions.

Our first observation is that the internal parameters typically change when a wound is present. This is a typical feature of living matter and not shared by ordinary inanimate matter where boundary conditions are not expected to influence the internal parameters of the system. Thus a jammed solid could possibly slowly invade a new open space and unjamming would eventually only occur because of a reduction of the density. In our case, however, the change of velocity distribution is instead compatible with a rapid change of internal parameters such as self-propulsion or alignment, way before the cell density is reduced. Once the parameters associated to each experiments have been determined, we are able to place them on a phase diagram reconstructed with the model. To this end, we perform numerical simulations of the active particle model under closed boundary conditions. The jamming phase can be identified considering the particle diffusion, quantified by the mean-square displacement [18]. We observe that the effective diffusion constant displays system size dependent effect in parameter space, allowing us to identify the transition point. As expected for second-order phase transitions, the curve describing the variation of the diffusion constant with control parameters and system size obeys finite size scaling. We can thus obtain scaling exponents by performing data collapse.

In our analysis of wound healing experiments, we have recorded parameters in steady-state conditions, disregarding the initial transient phase where the horizontal velocity builds up. Previous studies have shown that collective migration is associated with the propagation of waves of coordinated reorientation starting at the front [28, 29]. This is in line with our

observation of a change of parameters induced by the boundary and suggests that changes first occur at the wound site and then rapidly propagate inside the layer. The phenomenon of collective cell velocity reorientation in the direction of the wound has been explained considering cell guidance through intracellular force propagation in combination with the idea of plithotaxis, defined as the tendency for cells to move along the axis of maximal normal stress [30]. The presence of a wound suddenly decreases the local stress on the boundary cells, inducing internal changes that are then transmitted to the bulk cells, leading to the emergent unjamming of the entire monolayer.

Appendix A: Methods

Cell culture

HeLa cell line (ATCC CCL-2) is cultured as discussed in Ref. [10]. Cells are seeded in bovine soluble collagen, or fibrillar bovine collagen or without collagen-coated dishes and growth up to reach confluence overnight (see [10]) Endothelial cells derived from embryonic stem cells with homozygous null mutation of the VE-cadherin gene (VEC null) [23]. The wild type form of VE-cadherin was introduced in these cells (VEC positive) as described in detail in [24]. Endothelial cells isolated from lungs of wild type adult mice and cultured as previously described [10, 25]. The MCF-10A cell line is a non-tumorigenic human mammary epithelial cell line cultured as discussed in [13].

Wound healing assay

For the migration assay, a wound is introduced in the central area of the confluent cell sheet by using a pipette tip and the migration followed by time-lapse imaging. HeLa cells were stained with 10 μ M Cell tracker green CMFDA (Molecular Probes) in serum-free medium for 30 minutes and then the complete medium was replaced. Mouse endothelial cell monolayers were wounded after an overnight starving, washed with PBS, and incubated at 37°C in starving medium. MCF-10A cell monolayers were wounded after an O/N doxycycline induction, washed with PBS, and incubated at 37°C in fresh media+doxycycline.

Time lapse imaging

For HeLa cells, time-lapse multifield experiments were performed using an automated inverted Zeiss Axiovert S100 TV2 microscope (Carl Zeiss Microimaging Inc., Thornwood, NY) with a chilled Hamamatsu CCD camera OrcaII-ER. Displacements of the sample and the image acquisition are computer-controlled using Oko-Vision software (from Oko-lab). This Microscope was equipped with a cage incubator designed to maintain all the required environmental conditions for cell culture all around the microscopy workstation, thus enabling to carry out prolonged observations on biological specimens. Cell Tracker and Phase contrast images were acquired with an A-Plan 10x (NA 0.25) objective; the typical delay between two successive images of the same field was set to 10 minutes for 12 hours. For mouse endothelial cells and MCF-10A cells, time-lapse imaging of cell migration was performed on an inverted microscope (Eclipse TE2000-E; Nikon) equipped with an incubation chamber (OKOLab) maintained at 37°C in an atmosphere of 5% CO₂. Movies were acquired with a Cascade II 512 (Photometrics) charge-coupled device (CCD) camera controlled by MetaMorph Software (Universal Imaging) using a 4X or 10 magnification objective lens (Plan Fluor 10, NA 0.30). Images were acquired every 2 or 5 min over a 24h period. See Refs. [10, 13] for more details.

Particle image velocimetry (PIV)

The measurements of the velocity field were done using PIVlab app for Matlab [31, 32]. The method is based on the comparison of the intensity fields of two consequent photographs of cells. The difference in the intensity is converted into velocity field measured in $px/frame$ and then converted to $\mu m/h$ [10].

Fit of the experimental data

To find the values of simulation parameters that fit experimental data, extensive numerical simulations were performed to cover the parameter space. The main parameters to vary were β , σ_0 , F_0 , and, to less extent, α . Then the fitting was done for each experimental pair of values $\langle v_x \rangle_{exp}$ and Σ_{exp} , through the variable $M = ((\xi_{exp} - \xi_{sim})/\xi_{exp})^2 + \int dv (P_{exp}(v) - P_{sim}(v))^2 / \Sigma_{exp}$. The variable M was computed for a large number of simulations spanning

the parameter space and its minimum was selected as the best fit.

- [1] Peter Friedl and Darren Gilmour, “Collective cell migration in morphogenesis, regeneration and cancer,” *Nat Rev Mol Cell Biol* **10**, 445–57 (2009).
- [2] Olga Ilina and Peter Friedl, “Mechanisms of collective cell migration at a glance,” *J Cell Sci* **122**, 3203–8 (2009).
- [3] Dhananjay T Tambe, C Corey Hardin, Thomas E Angelini, Kavitha Rajendran, Chan Young Park, Xavier Serra-Picamal, Enhua H Zhou, Muhammad H Zaman, James P Butler, David A Weitz, Jeffrey J Fredberg, and Xavier Trepap, “Collective cell guidance by cooperative inter-cellular forces,” *Nat Mater* **10**, 469–75 (2011).
- [4] Agusti Brugues, Ester Anon, Vito Conte, Jim H. Veldhuis, Mukund Gupta, Julien Colombelli, Jose J. Munoz, G. Wayne Brodland, Benoit Ladoux, and Xavier Trepap, “Forces driving epithelial wound healing,” *Nat Phys* **10**, 683–690 (2014).
- [5] Anna Haeger, Marina Krause, Katarina Wolf, and Peter Friedl, “Cell jamming: collective invasion of mesenchymal tumor cells imposed by tissue confinement,” *Biochim Biophys Acta* **1840**, 2386–95 (2014).
- [6] Janina R Lange and Ben Fabry, “Cell and tissue mechanics in cell migration,” *Exp Cell Res* **319**, 2418–23 (2013).
- [7] Thorsten M Koch, Stefan Münster, Navid Bonakdar, James P Butler, and Ben Fabry, “3d traction forces in cancer cell invasion,” *PLoS One* **7**, e33476 (2012).
- [8] Thomas E Angelini, Edouard Hannezo, Xavier Trepap, Manuel Marquez, Jeffrey J Fredberg, and David A Weitz, “Glass-like dynamics of collective cell migration,” *Proc Natl Acad Sci U S A* **108**, 4714–9 (2011).
- [9] Jin-Ah Park, Jae Hun Kim, Dapeng Bi, Jennifer A Mitchel, Nader Taheri Qazvini, Kelan Tantisira, Chan Young Park, Maureen McGill, Sae-Hoon Kim, Bomi Gweon, Jacob Notbohm, Robert Steward, Jr, Stephanie Burger, Scott H Randell, Alvin T Kho, Dhananjay T Tambe, Corey Hardin, Stephanie A Shore, Elliot Israel, David A Weitz, Daniel J Tschumperlin, Elizabeth P Henske, Scott T Weiss, M Lisa Manning, James P Butler, Jeffrey M Drazen, and Jeffrey J Fredberg, “Unjamming and cell shape in the asthmatic airway epithelium,” *Nat Mater* **14**, 1040–1048 (2015).

- [10] Oleksandr Chepizhko, Costanza Giampietro, Eleonora Mastrapasqua, Mehdi Nourazar, Miriam Ascagni, Michela Sugni, Umberto Fascio, Livio Leggio, Chiara Malinverno, Giorgio Scita, Stéphane Santucci, Mikko J Alava, Stefano Zapperi, and Caterina A M La Porta, “Bursts of activity in collective cell migration,” *Proc Natl Acad Sci U S A* **113**, 11408–11413 (2016).
- [11] Xin Ye and Robert A Weinberg, “Epithelial-mesenchymal plasticity: A central regulator of cancer progression,” *Trends Cell Biol* **25**, 675–86 (2015).
- [12] Andrea J. Liu, Sidney R. Nagel, and J. S. Langer, “The jamming transition and the marginally jammed solid,” *Annu. Rev. Condens. Matter Phys.* **1**, 347–369 (2010).
- [13] Chiara Malinverno, Salvatore Corallino, Fabio Giavazzi, Martin Bergert, Qingsen Li, Marco Leoni, Andrea Disanza, Emanuela Frittoli, Amanda Oldani, Emanuele Martini, Tobias Lendenmann, Gianluca Deflorian, Galina V Beznoussenko, Dimos Poulikakos, Ong Kok Haur, Marina Uroz, Xavier Trepate, Dario Parazzoli, Paolo Maiuri, Weimiao Yu, Aldo Ferrari, Roberto Cerbino, and Giorgio Scita, “Endocytic reawakening of motility in jammed epithelia,” *Nat Mater* **16**, 587–596 (2017).
- [14] Dapeng Bi, J. H. Lopez, J. M. Schwarz, and M. Lisa Manning, “A density-independent rigidity transition in biological tissues,” *Nat. Phys.* **11**, 1074–+ (2015).
- [15] D. Weaire and J. P. Kermode, “Computer simulation of a two-dimensional soap froth ii. analysis of results,” *Philosophical Magazine B* **50**, 379–395 (1984), <https://doi.org/10.1080/13642818408238863>.
- [16] Tohru Okuzono and Kyozi Kawasaki, “Intermittent flow behavior of random foams: A computer experiment on foam rheology,” *Phys. Rev. E* **51**, 1246–1253 (1995).
- [17] Bo Li and Sean X Sun, “Coherent motions in confluent cell monolayer sheets,” *Biophys J* **107**, 1532–41 (2014).
- [18] Dapeng Bi, Xingbo Yang, M. Cristina Marchetti, and M. Lisa Manning, “Motility-driven glass and jamming transitions in biological tissues,” *Phys. Rev. X* **6**, 021011 (2016).
- [19] B. Szabó, G. J. Szöllösi, B. Gönci, Zs. Jurányi, D. Selmeczi, and Tamás Vicsek, “Phase transition in the collective migration of tissue cells: Experiment and model,” *Phys. Rev. E* **74**, 061908 (2006).
- [20] M Poujade, E Grasland-Mongrain, A Hertzog, J Jouanneau, P Chavrier, B Ladoux, A Buguin, and P Silberzan, “Collective migration of an epithelial monolayer in response to a model

- wound,” *Proc Natl Acad Sci U S A* **104**, 15988–93 (2007).
- [21] Néstor Sepúlveda, Laurence Petitjean, Olivier Cochet, Erwan Grasland-Mongrain, Pascal Silberzan, and Vincent Hakim, “Collective cell motion in an epithelial sheet can be quantitatively described by a stochastic interacting particle model,” *PLoS Comput Biol* **9**, e1002944 (2013).
- [22] Sri Ram Krishna Vedula, Andrea Ravasio, Chwee Teck Lim, and Benoit Ladoux, “Collective cell migration: a mechanistic perspective,” *Physiology (Bethesda)* **28**, 370–9 (2013).
- [23] G Balconi, R Spagnuolo, and E Dejana, “Development of endothelial cell lines from embryonic stem cells: A tool for studying genetically manipulated endothelial cells in vitro,” *Arterioscler Thromb Vasc Biol* **20**, 1443–51 (2000).
- [24] Maria Grazia Lampugnani, Adriana Zanetti, Ferruccio Breviario, Giovanna Balconi, Fabrizio Orsenigo, Monica Corada, Raffaella Spagnuolo, Martha Betson, Vania Braga, and Elisabetta Dejana, “Ve-cadherin regulates endothelial actin activating rac and increasing membrane association of tiam,” *Mol Biol Cell* **13**, 1175–89 (2002).
- [25] Costanza Giampietro, Andrea Disanza, Luca Bravi, Miriam Barrios-Rodiles, Monica Corada, Emanuela Frittoli, Cecilia Savorani, Maria Grazia Lampugnani, Barbara Boggetti, Carien Niessen, Jeff L Wrana, Giorgio Scita, and Elisabetta Dejana, “The actin-binding protein eps8 binds ve-cadherin and modulates yap localization and signaling,” *J Cell Biol* **211**, 1177–92 (2015).
- [26] Simon Garcia, Edouard Hannezo, Jens Elgeti, Jean-François Joanny, Pascal Silberzan, and Nir S Gov, “Physics of active jamming during collective cellular motion in a monolayer,” *Proc Natl Acad Sci U S A* **112**, 15314–9 (2015).
- [27] Thomas E Angelini, Edouard Hannezo, Xavier Trepat, Jeffrey J Fredberg, and David A Weitz, “Cell migration driven by cooperative substrate deformation patterns,” *Phys Rev Lett* **104**, 168104 (2010).
- [28] Assaf Zaritsky, Doron Kaplan, Inbal Hecht, Sari Natan, Lior Wolf, Nir S Gov, Eshel Ben-Jacob, and Ilan Tsarfaty, “Propagating waves of directionality and coordination orchestrate collective cell migration,” *PLoS Comput Biol* **10**, e1003747 (2014).
- [29] Assaf Zaritsky, Erik S Welf, Yun-Yu Tseng, M Angeles Rabadán, Xavier Serra-Picamal, Xavier Trepat, and Gaudenz Danuser, “Seeds of locally aligned motion and stress coordinate a collective cell migration,” *Biophys J* **109**, 2492–500 (2015).

- [30] Xavier Trepap and Jeffrey J Fredberg, “Plithotaxis and emergent dynamics in collective cellular migration,” *Trends Cell Biol* **21**, 638–46 (2011).
- [31] William Thielicke, *The flapping flight of birds: Analysis and application*, Ph.D. thesis (2014).
- [32] W. Thielicke and E.J. Stamhuis, “Pivlab – towards user-friendly, affordable and accurate digital particle image velocimetry in matlab,” **2** (2014), 10.5334/jors.bl.

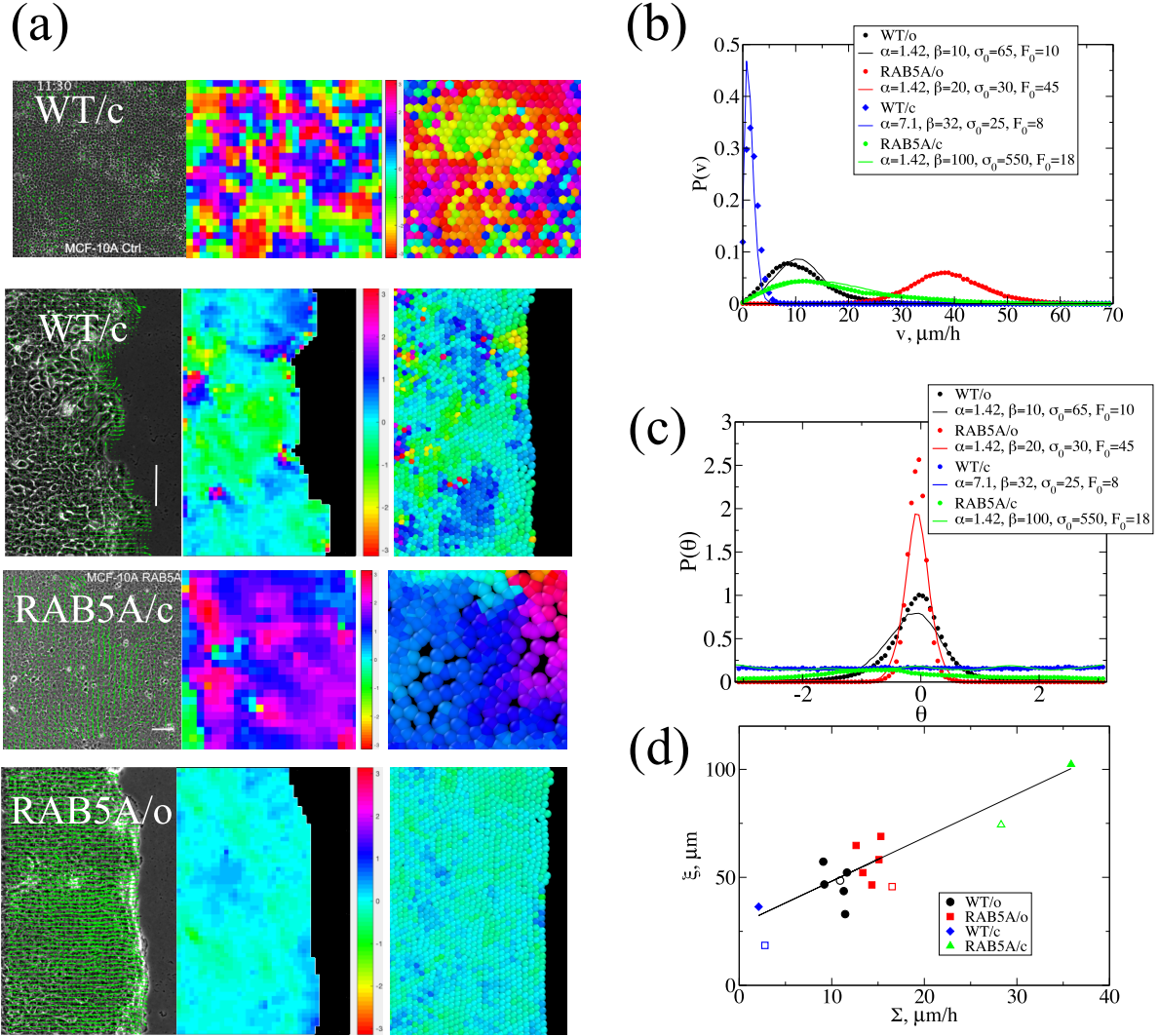


FIG. 1. Statistical properties of collective migration in epithelial cells. a) Velocity maps obtained from PIV for WT MCF-10A cells in wound healing (WT/o) and confluent (WT/c) conditions, as well as MCF-10A cells with RAB5A overexpression under the same conditions (RAB5A/o and RAB5A/c, respectively). Arrows represent the velocities and the color their orientations. Experimental results are compared with simulations. b) The distribution of the absolute values of the velocities for the experiments reported in panel a) compared with the corresponding simulation results. c) Distribution of velocity orientations for the same cases. d) Velocity correlation length ξ_c as a function of the velocity fluctuations Σ . The linear regression was predicted by an earlier model [26].

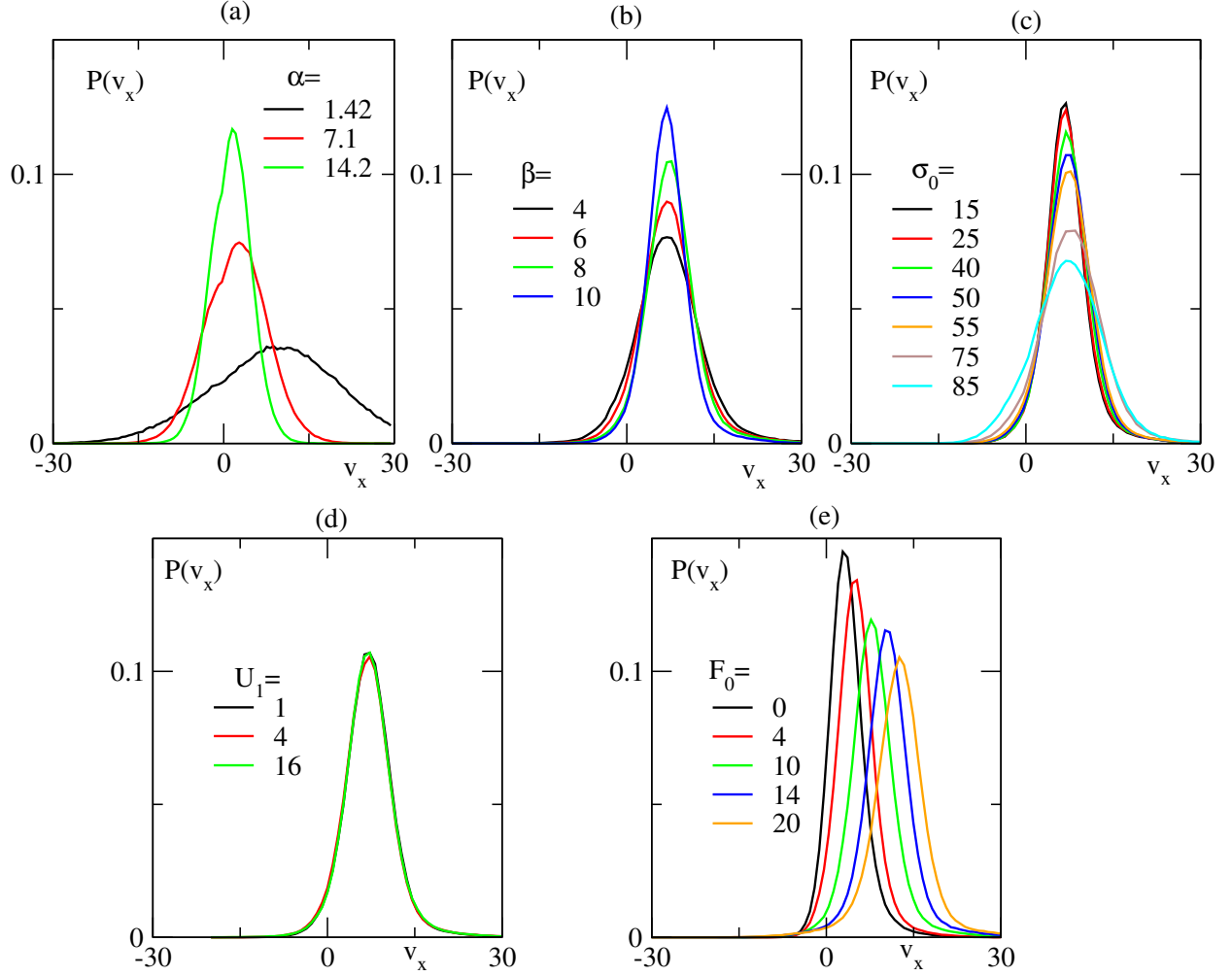


FIG. 2. Effect of the model parameters on the cell velocity distribution. Effect of a) damping α , b) alignment strength β , c) noise σ_0 , d) adhesion U_0 and e) self-propulsion force F_0 on $P(v_x)$, where v_x is the velocity in the invasion direction in wound healing conditions.

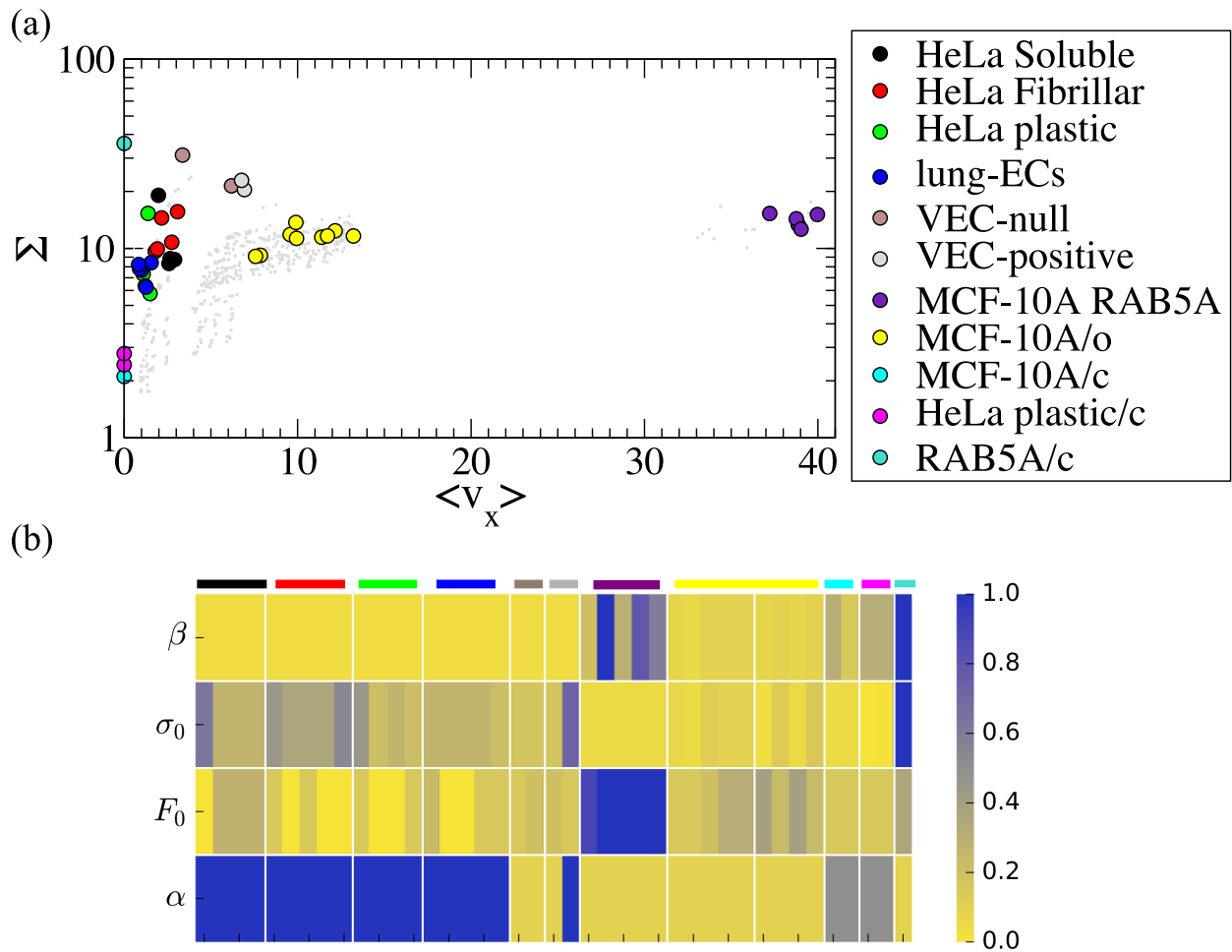


FIG. 3. The parameter space of cell migration. a) A map of the average velocity in the invasion direction $\langle v_x \rangle$ and the velocity standard deviation Σ for all the cell lines analyzed. b) A colormap of the best parameters β , F_0 , σ_0 and α obtained by comparing each experiment with simulations. The color scale is normalized separately for each parameter (with $\beta^{\max} = 100$, $F_0^{\max} = 50$ and $\sigma_0^{\max} = 400$ and $\alpha^{\max} = 14.2$) Each column represents an experiment with a cell line associated with the color legend.

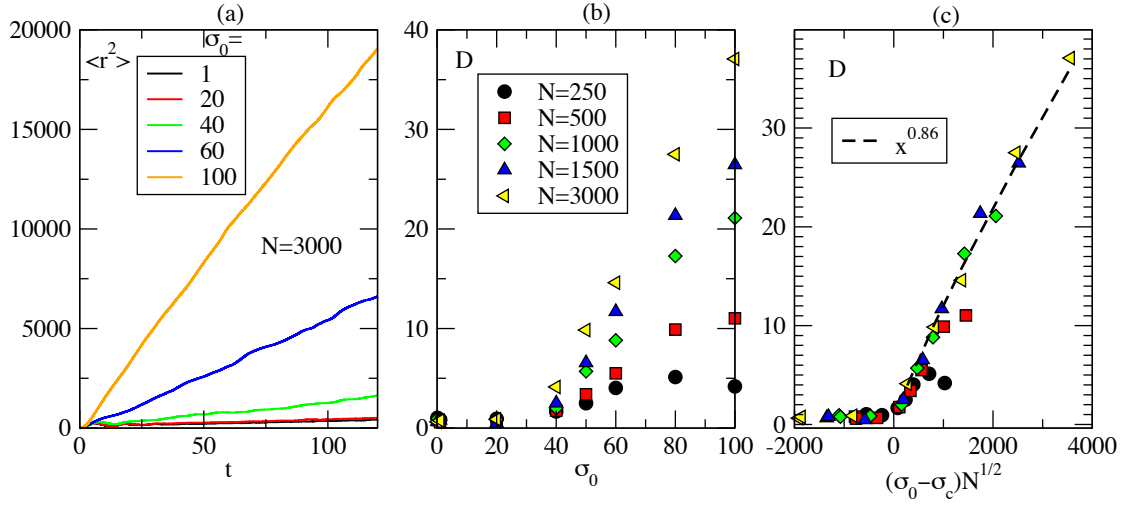


FIG. 4. Characterization of the jamming-flowing transition in a simulated confluent layer. a) The time dependence of the mean-square displacement as a function of the noise amplitude σ_0 b) The diffusion constant displays a system-size dependent behavior above a noise level σ_c that can be used to identify the jamming point. c) The curves from panel b) can be collapsed assuming a finite-size scaling form.

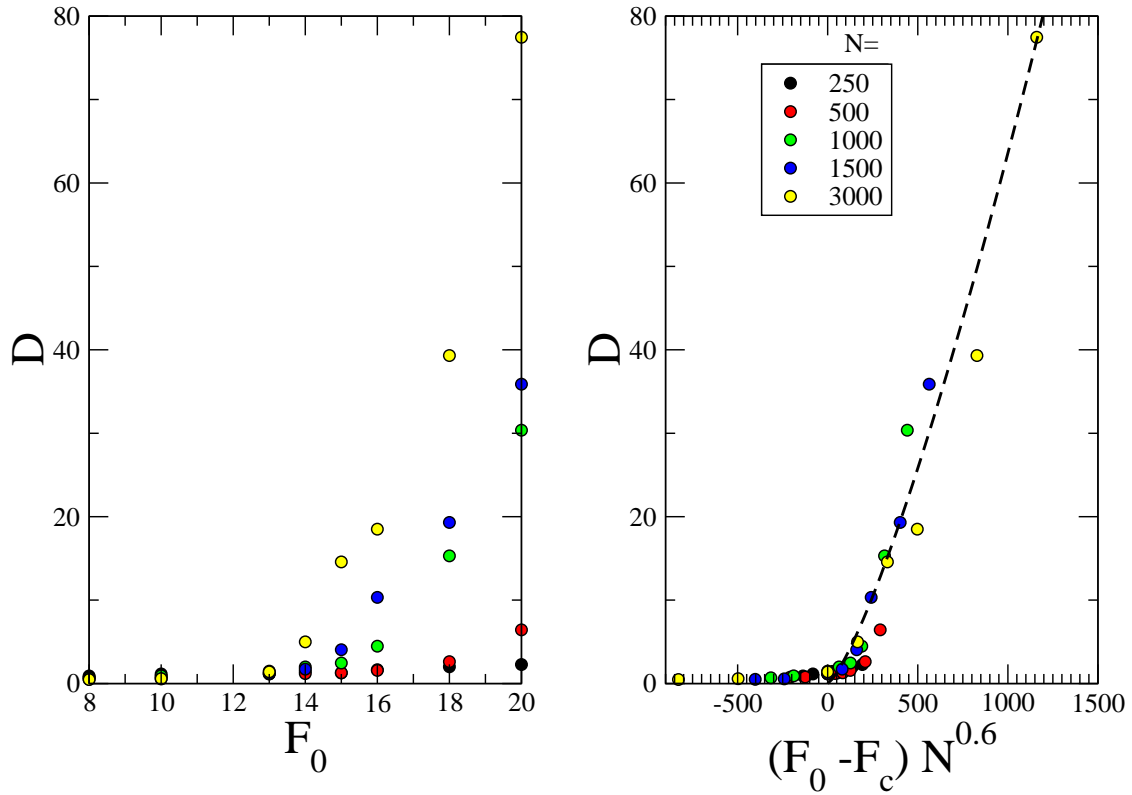


FIG. 5. a) The diffusion constant as a function of the self-propulsion force F_0 displays a system-size dependent behavior above a noise level F_c that can be used to identify the jamming point. b) The curves from panel a) can be collapsed assuming a finite-size scaling form.

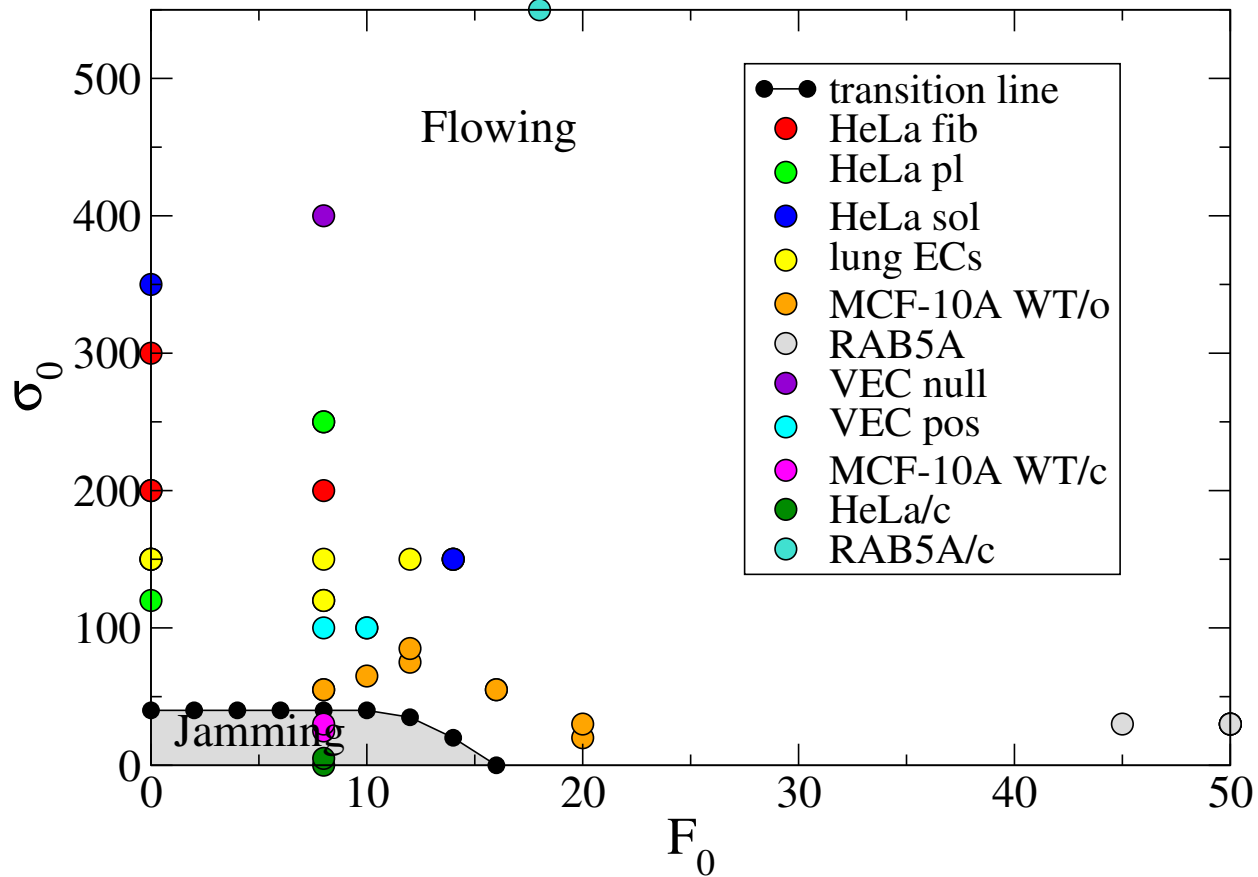


FIG. 6. The jamming phase diagram. A projection of the jamming phase diagram on the (σ_0, F_0) plane, for $\beta = 10$ and $\alpha = 1.4$. For each experiment, we report on the phase diagram the best estimate for σ_0 and F_0 . Experiments performed in confluent conditions are all in the jamming phase, those in wound healing conditions are mostly in the flowing phase.